New Journal of Physics
The open access journal at the forefront of physics

Deutsche Physikalische Gesellschaft DPG IOP Institute of Physics

PAPER • OPEN ACCESS

Physics of rowing oars

To cite this article: Romain Labbé *et al* 2019 *New J. Phys.* **21** 093050

New Journal of Physics
The open access journal at the forefront of physics

Deutsche Physikalische Gesellschaft DPG
IOP Institute of Physics

Published in partnership with: Deutsche Physikalische Gesellschaft and the Institute of Physics

OPEN ACCESS

RECEIVED
11 April 2019

REVISED
31 July 2019

ACCEPTED FOR PUBLICATION
6 September 2019

PUBLISHED
24 September 2019

PAPER

Physics of rowing oars

Romain Labbé[1,2], **Jean-Philippe Boucher**[1,2], **Christophe Clanet**[1] **and Michael Benzaquen**[1]

[1] LadHyX, UMR CNRS 7646, Ecole polytechnique, F-91128 Palaiseau Cedex, France
[2] Phyling, 73 rue Léon Bourgeois, F-91120 Palaiseau, France

E-mail: michael.benzaquen@polytechnique.edu

Keywords: sports physics, rowing, optimization, oars

Abstract

In each rowing sport (rowing, kayaking, canoeing), the oars have their very own characteristics most of the time selected through a long time experience. Here we focus on rowing and address experimentally and theoretically the problem of rowing efficiency as function of oar lengths and blades sizes. In contrast with previous studies which consider imposed kinematics, we set an imposed force framework which is closer to human constraints. We find that optimal oar lengths and blades sizes depend on sports and athletes strength, and we provide an optimization scheme.

1. Introduction

Most sports require different equipment for different weight categories and genders. For example, in shot put, women use masses of 4 kg, while men use masses of 7.5 kg. However in rowing [1, 2], oar characteristics are rather constant in each discipline regardless of athletes strength and gender. In *sculling* (figure 1(a)), the oar size ranges from 275 cm for short *Fat2 Blade* to 292 cm for long *Big Blade* [3, 4]. For sweep boats (figure 1(b)), the oar size reads 362–378 cm [3, 4]. Through rowing history, the tendency has been to reduce oar lengths (by almost 25% since 1850, see figures 2(a) and (c)). This evolution is also related to an increase in the blade area and the shift to asymmetric blades (figures 2(b) and (e)). While not being the only improving factors, these changes have likely contributed to the increase of performance over time (figure 2(d)).

In rowing competitions, the average stroke rate ranges between 30 and 40 strokes per minute depending on the boat category[3], which corresponds to strokes of 1.5–2 s. At the beginning of the race, the stroke rate is yet much higher (40–45 strokes per minute for a single scull and 45–50 for a coxless four) [8]. The rowing stroke is divided into two phases: a propulsive phase of about 0.7 s (40% of the stroke) and a recovery phase of 1.1 s (60% of the stroke) [9]. During the propulsive stroke, typical force profiles exerted by the blade on the water were measured by Valery Klesnev [10] and are reprinted in figure 3(a). As one can see, the maximal handle force exerted is around 700 N. Our study is conducted in the limit of a constant force profile, which corresponds to the first order approximation of the actual force profile. As we shall see, this approximation allows us to gain further understanding on the effects of oars' length and blade size. Beyond this approximation, the framework we provide allows to use more accurate force profiles and to compute the resulting dynamics numerically. Also note that the force does remain rather constant during the whole race, as evidenced from the rather constant stroke frequency revealed in figure 3(b).

The main problem in rowing is the determination (and optimization) of the mean velocity of the hull which results from a balance between propulsion and friction. The question of friction has been addressed by Wellicome in 1967 [11] for the steady motion and rediscussed lately by Day *et al* [12] to account for unsteadiness. The propulsion phase is more debated as underlined in the review of Caplan in 2010 [13]. All authors agree that the initial acceleration phase is dominated by drag [14] but once the boat reaches its steady motion lift plays a role [15, 16] as well as the elasticity of the shaft [17–19]. Theoretically, most of the studies are developed in the footprints of the pioneering work of Alexander [20] and show that observations can be satisfactorily approached with a one dimensional momentum balance, infinitely stiff oars with inertia and non-infinitesimal stroke angles, and quadratic relationships between force and

[3] The average stroke rate is about 33–35 strokes per minute for a single scull and 39 for a coxless four.

Figure 1. Front view of a single scull (a) and a coxless pair (b) [1, 2]. The inboard and outboard lengths are respectively denoted ℓ and L. Typical lengths are indicated. (a) © FFA — Daniel Blin, (b) © FFA — Mimmo Perna.

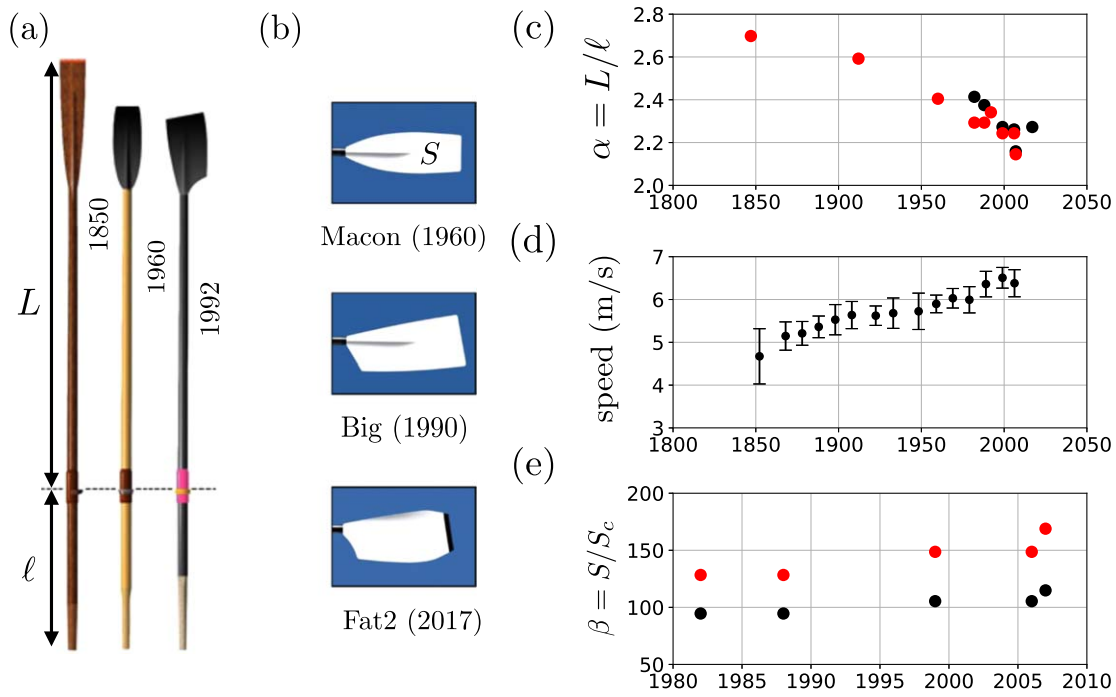

Figure 2. (a) Picture of three different sweep oars (This SquareMaconCleaver image has been obtained by the author(s) from the Wikimedia website where it was made available Yeti Hunter under a CC BY-SA 2.0 licence. It is included within this article on that basis. It is attributed to Yeti Hunter.). The left oar dates back to 1850, the middle one to 1960, and the right one to 1992. (b) Pictures, from top to bottom, of a *Macon Blade* (1960), a *Big Blade* (1990) and a *Fat2 Blade* (2017) (Reproduced with permission from [3]. © Concept2, Inc). (c) Evolution of the oar aspect ratio $\alpha = L/\ell$ for sculling oars in black and sweep oars in red. Note that since the inboard length ℓ remained quite constant through time, α can be seen as the dimensionless oar length. The oldest data points were obtained from race photographs, while the more recent ones come from [6] or were provided by the French athlete Thomas Baroukh. (d) Evolution of the mean speed of the winner boat at the Oxford and Cambridge Boat Race (data gathered from [7]). (e) Evolution of the dimensionless blade area $\beta = S/S_c$ with S the blade area and $S_c = S_h C_h/(NC_d)$, where N is the number of blades, C_d the drag coefficient of a blade, S_h the hull wetted surface and C_h the hull drag coefficient (for all the points, the hull wetted surface is taken constant as that of a coxless four rowing boat $S_h = 5.92\ m^2$). The black dots are for sculling blades and red dots for sweep blades. Data come from [6].

velocity for the boat and oar blade [21]. We will follow those footprints to develop our model. Concerning the effect of oars' length, Nolte [6] performed an empirical study on a dataset of rowing races. He reported that 'Shorter Oars Are More Effective'. However, Laschowski *et al* [22] studied experimentally the effect of oar-shaft stiffness and length with elite athletes. They showed that changes in stiffness and oars' length led to small differences in the measured boat acceleration but these differences remained of the same order of magnitude as inter-stroke fluctuations. To get a clear answer on the question we decided to avoid the fluctuations induced by humans and developed a rowing robot.

In section 1, we present the methods of this study with the design of the rowing robot. Section 2 is dedicated to the experimental results. In section 3, we first derive the dynamical equations for a rigid oar. We then compute the boat velocity at given imposed force for varying oar lengths and compare our results to experiments. Finally,

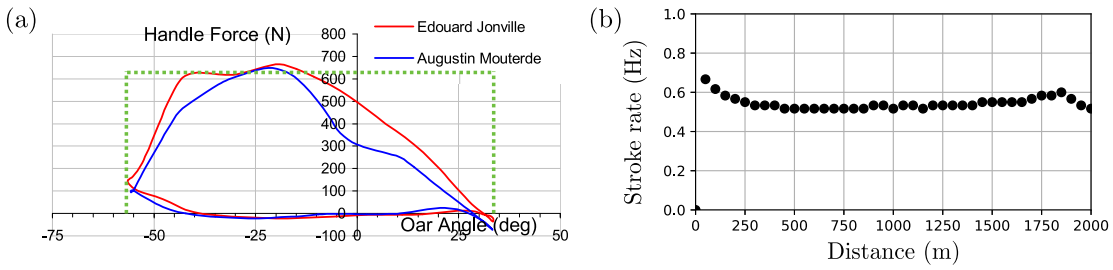

Figure 3. (a) Handle force during one stroke as a function of the oar angle for two top-level French rowers (Edouard Jonville and Augustin Mouterde). These data were collected by Valery Klesnev [10]. A 0° oar angle corresponds to oars perpendicular to the boat. (b) Typical stroke frequency during a rowing race, specifically the Lucerne 2016 world championship for the winner boat in the M1x category (data extracted from [8]).

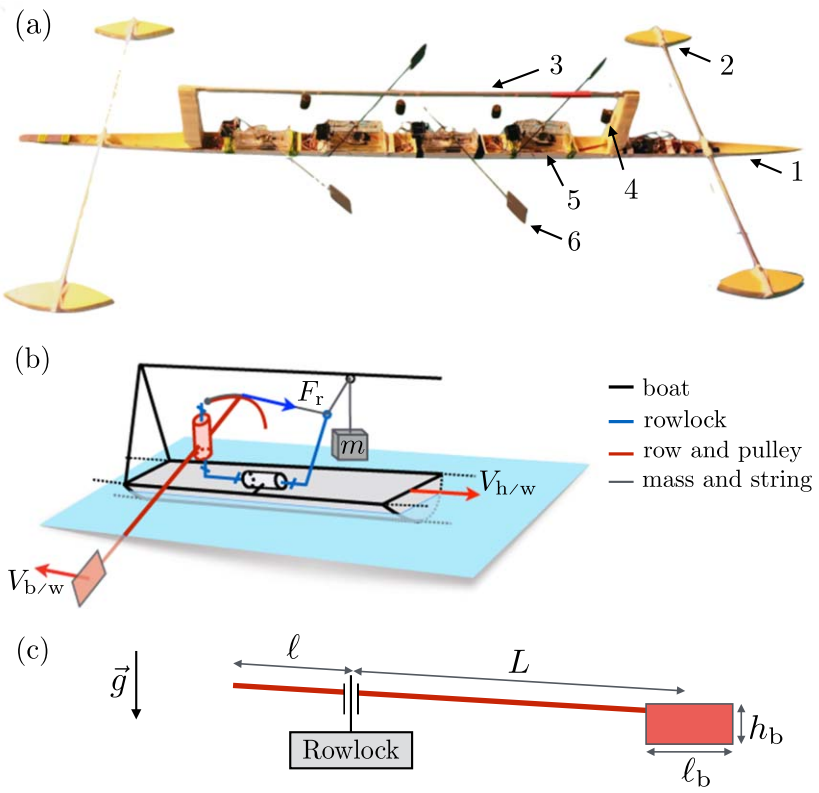

Figure 4. (a) Picture of the 2 m long model rowing boat with 4 robot rowers at constant force with (1) a hull, (2) 4 floats, (3) a mass support, (4) 4 masses of 80 g, (5) 4 robot rowers and (6) 4 oars. (b) Sketch of the mechanism of one robot rower. The oar and pulley (red) rotate with respect to the rowlock (blue), itself in rotation with respect to the hull (black) to ensure lifting/dropping of the oar between the propulsive and recovery phases. A suspended mass/string system (gray) ensures oar motion at constant force during the propulsive phase. The recovery phase and the blade flips were ensured by two servomotors and position sensors connected to an Arduino™ board (not shown for clarity). (c) Side view sketch of the oar/rowlock system.

we present master plots on the efficiency of rowing boats and discuss the particular case of sweep oars optimization. In section 4 we conclude.

2. Methods: rowing robot at constant force

In order to understand the effect of the ratio $\alpha = L/\ell$ on the boat speed in the limit of constant force, we designed and manufactured a rowing robot with imposed propulsive force (see figure 4). Using a home-made wooden mold based on a real rowing shell [23] at the scale 1/10th, we built a glass fiber rowing boat (see figure 4(a)(1)) with 4 robot rowers (figure 4(a)(5)) using one oar each (figure 4(a)(6)). Constant force during the propulsive phase was ensured through a pulley-mass system. Each oar was linked to a pulley centered at its rowlock. A suspended mass $m = 80$ g (see figure 4(a)(4)) was connected to the pulley through a string

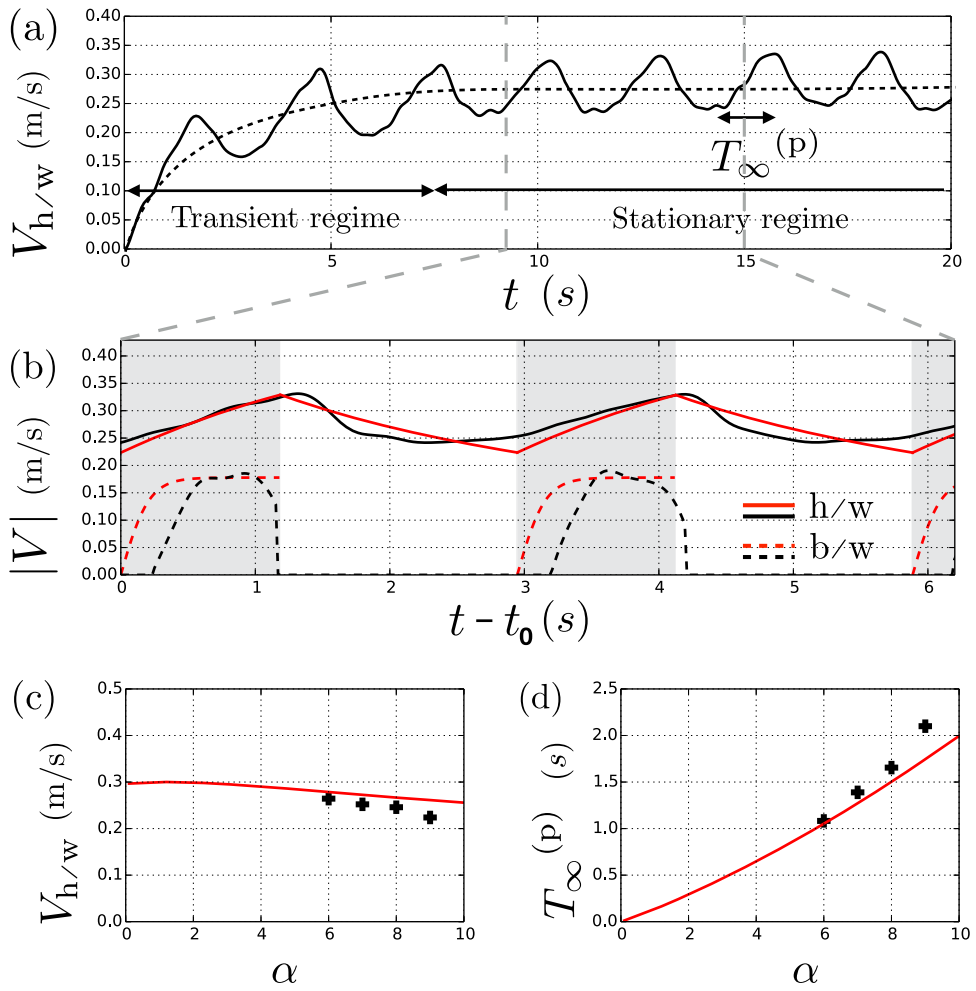

Figure 5. (a) Instantaneous velocity (solid lines) and mean velocity (dash line) of the hull with respect to the water, starting from rest at $t = 0$, for $\alpha = 7$. (b) Velocity of the hull with respect to the water (solid lines) and absolute velocity of the blade (dash line) with respect to the water as function of time over two consecutive rowing cycles in the stationary regime, for $\alpha = 7$, theory (equations (9)–(12)) in red and experiments in black. (c) Mean boat velocity and (d) propulsive stroke duration as function of α, black crosses signify experiments while solid red lines indicate theoretical predictions, equations (9)–(12).

(see figure 4(b)) by that setting the oar in motion at constant force $F_r = mg$ (if we neglect frictional losses in all connections). Consistent with actual data which reveals a catch angle of $\approx -55°$ and finish angle of $\approx 35°$ (see figure 3(a)), the angular travel of the oar was fixed to $\theta_0 = 90°$ [4]. The recovery phase and the blade flips were ensured by two servomotors and position sensors connected to an Arduino™ board. The masses are suspended to a unique support (see figure 4(a)(3)) and the stability of the boat was ensured by four polystyrene floats (see figure 4(a)(2)).

The experiments were performed at the swimming pool of Ecole polytechnique. Setting the recovery phase time to a constant value $T^{(r)} = 1.3$ s (such that it roughly matches empirical conditions: 40% propulsion against 60% recovery), we video recorded the model rowing boat over 25 m for four different oar lengths, with corresponding aspect ratios spanning from $\alpha = 5$ to $\alpha = 8$.

3. Results

As one can see in figure 5(a) after the start, the speed of the hull $V_{h/w}$ increases during about 8 s (3 strokes) until it reaches a stationary regime where the average speed remains constant. Stationary stroke duration $T_\infty^{(p)}$ was recorded for each stroke using the position sensors mentioned above and averaged for each race.

In figure 5(b), the time evolution of the hull and blade velocities in the stationary regime are plotted (black curve). One can easily distinguish two phases: the propulsive phase where the hull speed increases and the recovery phase where the speed decreases. Note that in reality, the speed keeps increasing at the beginning of the recovery stroke due to the motion of the rowers on the boat [24]. The experiments show that, for a given force, when increasing α, the average hull velocity $\overline{V_{h/w}}$ decreases (black dots in figure 5(c)), coherent with an increase

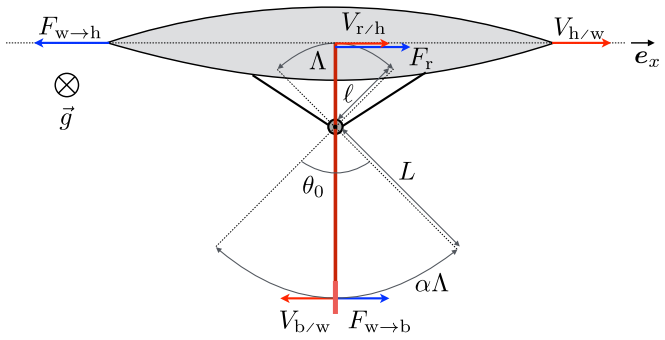

Figure 6. Top view sketch of a model rowing boat (for clarity, only one oar/rowlock system is depicted). Forces are presented in blue and velocities in red.

in the propulsive stroke duration $T_\infty^{(p)}$ (see figure 5(d)). This observation agrees quite well with the historical evolution of the ratio α for real oars, presented in figure 2(c), as α decreased over the years with faster and faster boats (see figure 2(d)).

4. Discussion

4.1. Dynamics of a rigid oar

Here, we present the dynamical equations that govern oar propulsion for a given force profile exerted by the rower. The first kinematic relation relating the velocities in the different reference frames reads (see figure 6):

$$V_{b/w} = V_{b/h} + V_{h/w}, \tag{1}$$

where $V_{b/w}$, $V_{b/h}$ and $V_{h/w}$ respectively denote the speed of the blade with respect to the water, the speed of the blade with respect to the hull, and the speed of the hull with respect to the water[4]. The second kinematic relation ensures conservation of angular momentum of the oar at the oarlock (see figure 6):

$$V_{b/h} = -\alpha V_{r/h}, \tag{2}$$

where $V_{r/h}$ denotes the speed of the rower hands in the reference frame of the hull and $\alpha = L/\ell$ is the ratio between the outboard and inboard lengths. To reach analytical predictions we use the 1D theoretical framework developed by Cabrera *et al* in 2006 [21]. From now on, we assume that $V_{b/w}$ and $V_{b/h}$ are all parallel to the direction of motion of the hull, so we write in the small angle approximation: $V_{b/w} = V_{b/w}\,\boldsymbol{e}_x$ and $V_{b/h} = V_{b/h}\,\boldsymbol{e}_x$, together with $V_{h/w} = V_{h/w}\,\boldsymbol{e}_x$ and $V_{r/h} = V_{r/h}\,\boldsymbol{e}_x$, with $\boldsymbol{e}_x$ the unit vector in the direction of motion of the boat. The forces exerted on the moving blade are (i) the pressure drag F_p, and (ii) the added mass F_{am}, both parallel to the blade motion in the reference frame of the water (see [14, 25]):

$$F_p = -\frac{1}{2}\rho S C_d |V_{b/w}| V_{b/w}, \tag{3a}$$

$$F_{am} = -\rho \Omega C_m \dot{V}_{b/w}, \tag{3b}$$

where ρ denotes the water density, $S = \ell_b\, h_b$ is the surface of the blade, C_d and C_m are the drag and added mass coefficients, and $\Omega = \pi S \ell_b/4$ is the volume of the cylinder with diameter ℓ_b and height h_b (figure 4(c)). Note that we neglect here all contributions related to lift forces on the blade[5]. The net force $F_{w\to b} = F_p + F_{am}$ exerted by the water on the blade must match that of the rower F_r through a torque conservation relation at the rowlock (assuming the oar tubes to be rigid and of negligible mass). That is:

$$F_{w\to b} = \frac{1}{\alpha} F_r. \tag{4}$$

In the following, we choose to work on a simple and analytically solvable case by assuming a constant imposed force (figure 3(a)). Although previous studies (see [26, 28, 29]) show evidence of slightly time-dependent force profiles, we here wish to extract the general physics and scaling arguments of rowing mechanics with minimal ingredients, for which a constant force seems appropriate from a physiological point of view. Indeed, what the sportsman controls is rather the deployed force than the velocity which is nothing but the response of the physical system.

[4] The velocity of the blade that we consider here is the velocity at the center point of the blade (where the hydrodynamic force is exerted).

[5] Although lift might not be negligible especially during the beginning and the end of the rowing stroke [26, 27], it has the same scaling as the drag force and thus taking it into account would not significantly change our results.

4.2. Boat propulsion at constant force

Appendix shows a complete analysis of the oar dynamics for a resting hull with respect to the water and identifies two regimes depending on which drag component (added mass or pressure drag) is dominant. In this section we relax the constraint of an immobile hull ($V_{h/w} \neq 0$) and use the results of appendix to compute propulsion characteristics. At this point, the equation needed to close the problem results from the force balance on the hull. This is $F_{w\to h} = NF_r/\alpha$, with N the number of blades. We assume that the drag force on the hull is dominated by skin friction[6] and we do not take into account the motion of the rowers on the boat. According to Newton's second law, one obtains in this limit:

$$M\dot{V}_{h/w} + 1/2\rho S_h C_h |V_{h/w}| V_{h/w} = NF_r/\alpha, \tag{5}$$

where M is the total mass of the boat, S_h the wetted surface of the hull and C_h its skin drag coefficient. We use the hull parameters to non-dimensionalise the problem. Thus, we introduce the velocity scale $V^\star = \sqrt{2NF_c/(\rho S_h C_h)}$ and the time scale $\tau^\star = M\sqrt{2/(\rho NF_c S_h C_h)}$ and we write $V = \tilde{V}V^\star$, $t = \tilde{t}\tau^\star$ and $F = \tilde{F}F_c$, with F_c a characteristic force scale. The natural characteristic length of the problem is $L^\star = V^\star\tau^\star$. The dimensionless equation governing the boat velocity then writes:

$$|\tilde{V}_{h/w}|\tilde{V}_{h/w} + \dot{\tilde{V}}_{h/w} = \frac{1}{\alpha}\tilde{F}_r. \tag{6}$$

The dimensionless equation governing the dynamics of the oar (see equation (A.1) in appendix) reads:

$$\beta|\tilde{V}_{b/w}|\tilde{V}_{b/w} + \gamma\dot{\tilde{V}}_{b/w} = -\frac{1}{\alpha}\tilde{F}_r, \tag{7}$$

where:

$$\beta = NSC_d/(S_h C_h) \tag{8}$$

denotes the ratio between the blades' pressure drag and the hull skin drag and $\gamma = N\rho\Omega C_m/M$ is the ratio between the blades' added mass and the boat mass. In the following and for the sake of simplicity, we consider self-similar blades (ratio h_b/ℓ_b constant), so that $\gamma \sim \beta^{3/2}$, by that reducing the number of dimensionless parameters.

Each rowing cycle k is made of two phases: (i) the propulsive phase at constant force with duration $T_k^{(p)}$ for which we set $\tilde{F}_r = 1$ and (ii) the recovery phase with duration $T_k^{(r)}$ for which $\tilde{F}_r = 0$. The overall cycle period reads $T_k = T_k^{(p)} + T_k^{(r)}$. In the following, we shall restrict to a constant and prescribed duration for the recovery phase $T_k^{(r)} = T^{(r)}$ [7]. The solution of equation (6) reads in the propulsive phase ($\tilde{t} \in [\tilde{t}_k,\ \tilde{t}_k + \tilde{T}_k^{(p)}]$ with $\tilde{t}_k = k\tilde{T}_k$):

$$\tilde{V}_{h/w}^{(p)}(\tilde{t}) = \frac{1}{\sqrt{\alpha}}\tanh\left[\frac{1}{\sqrt{\alpha}}(\tilde{t} - \tilde{t}_k) + \tanh^{-1}[\tilde{V}_{h/w}^{(p)}(\tilde{t}_k)\sqrt{\alpha}\ ]\right], \tag{9}$$

and in the recovery phase ($\tilde{t} \in [\tilde{t}_k + \tilde{T}_k^{(p)},\ \tilde{t}_{k+1}]$):

$$\tilde{V}_{h/w}^{(r)}(\tilde{t}) = \frac{1}{(\tilde{V}_{h/w}^{(p)}(\tilde{t}_k + \tilde{T}_k^{(p)}))^{-1} + (\tilde{t} - \tilde{t}_k - \tilde{T}_k^{(p)})}. \tag{10}$$

To close the system, one needs the continuity equation for the velocity:

$$\tilde{V}_{h/w}^{(r)}(\tilde{t}_{k+1}) = \tilde{V}_{h/w}^{(p)}(\tilde{t}_{k+1}), \tag{11}$$

and the equation for the stroke duration $T_k^{(p)}$ of the kth propulsive phase:

$$\int_{t_k}^{t_k+T_k^{(p)}} V_{b/h}\,dt = \int_{t_k}^{t_k+T_k^{(p)}} (V_{b/w} - V_{h/w})\,dt = -\alpha\Lambda. \tag{12}$$

In order to test our theory, we compare its predictions with the results for our rowing robot with imposed propulsive force presented in the section 2 (see figure 4). The experimental results are reported in figure 5 and compared to the theoretical predictions of our model. The estimation of the oar parameters C_d and C_m is detailed in appendix. The drag coefficient on the hull C_h was estimated by measuring the deceleration of the fully loaded model boat with a given initial velocity and blades out of the water (we found $S_h\,C_h = (2.2 \pm 0.1)10^{-3}\,m^2$).

The measured instantaneous hull velocity (figure 5(b)) is found in quite good agreement with the theoretical predictions. The stroke duration (figure 5(d)) and the mean velocity (figure 5(c)) are slightly off the theoretical curves. These small discrepancies can be the results of two different effects. First, our model does not account for

[6] The skin friction is expected to account for 80% of the overall drag [26, 30]. Thus, we neglect here the other contributions to the drag on the boat (form drag, wave drag and aerodynamic drag).

[7] Note that another possible choice would be to set $T_k^{(r)} = T_k^{(p)}$.

the dynamic inclination of $F_{w\to b}$ with respect to the direction of motion of the boat, by that overestimating the propulsive force. Indeed the instantaneous real propulsive force should read $F_{w\to b}\cos\theta$ where $\theta\in[-\theta_0/2, \theta_0/2]$ denotes the angle of the oar with respect to the normal to the direction of motion. Although we do not wish to increase the model's complexity further by accounting for this effect, the associated correction can be roughly estimated by $\langle\cos\theta\rangle_{[-\theta_0/2,\theta_0/2]}\approx 10\%$. Second, our robot rowing boat suffered from an abrupt slow down at the end of the propulsive phase (figure 5(b)) due to both (i) the oars hitting the mechanical stop before being lifted out of the water, and (ii) the deceleration of the masses increasing the drag on the hull. Note that, in contrast with the static boat experiments of appendix, our model boat lies on the crossover between the added mass and pressure drag dominated regimes. Indeed, as can be seen on figure 5(b), the blade velocities display roughly balanced acceleration and plateau timescales. This key effect is precisely due to relaxing the static constraint by that shortening the blade's travel with respect to the water.

To interpret the results in term of efficiency, we define the *anchoring* $\mathcal{A}$ of the blade, as the ratio of the distance traveled by the hull during the propulsive phase, denoted $\Lambda_h(\alpha)$, and the travel of the blade in the reference frame of the boat $\alpha\,\Lambda$ (see figure 6):

$$\mathcal{A}=\frac{\Lambda_h}{\alpha\Lambda},\ \text{with}\ \Lambda_h(\alpha)=\int_0^{T_\infty^{(p)}} V_{h/w}\,dt. \tag{13}$$

The anchoring can be seen as the oar efficiency. Indeed, if $\mathcal{A}=1$, the blade does not move with respect to the water and all the rower's energy is transferred to the boat. In contrast, if $\mathcal{A}=0$ the boat does not move and the oars slip in the water. Interestingly the *anchoring* has an energetic interpretation. The propulsive energy provided by the rower $E_r=\Lambda\,F_r$ is dissipated by both the hull $E_h=\Lambda_h F_r/\alpha$ and the blades E_b, such that $E_r=E_h+E_b$. Equation (13) yields:

$$\mathcal{A}=\frac{E_h}{E_r}, \tag{14}$$

that is: the anchoring $\mathcal{A}\in[0,\,1]$ quantifies the efficiency of energy transfer between the rower and the boat [9, 31].

The tendencies and the optimization are discussed in the following section and compared to real rowing boat data.

4.3. Physical discussion

Here, we discuss the global optimization problem as function of parameters α and β and confront our results to real rowing boats. Figure 7 displays the dimensionless hull velocity, the stroke duration and the anchoring as function of α and β[8], together with a few 2D cuts to simplify the discussion. The velocity plot can be understood from the stroke duration and anchoring plots through the relation:

$$V\sim\frac{\mathcal{A}\alpha\Lambda}{T_\infty^{(p)}}. \tag{15}$$

At constant α, the rescaled velocity and the stroke duration are increasing functions of β (figures 7(a3) and (b3)) and saturate at large β. This can be understood through the anchoring behavior (figure 7(c3)). At small β—small blades—the anchoring is weak and much of the energy is dissipated by the blades motion with respect to the water. At large β, the large blades are well anchored in the water ensuring maximal energy transfer to the boat, or equivalently that the hull velocity matches the blade velocity with respect to the boat. The behavior with α at constant β is less trivial. The stroke duration is an increasing function of α and the velocity crosses over from a plateau at small α (added mass dominated) to an $\alpha^{-1/2}$ regime (pressure drag dominated) at large α. At large given β the anchoring is maximal ($\mathcal{A}\to 1$) and the velocity is a monotonous function of α, while for small given β there exists an optimal value of α that maximizes the velocity.

The mean power injected by a rower at constant maximal force writes:

$$\bar{P}=\frac{1}{T_\infty^{(p)}}\int_0^{T_\infty^{(p)}} F_r V_{h/w}\,dt=\frac{F_r\Lambda}{T_\infty^{(p)}} \tag{16}$$

$\bar{P}$ scales as $1/T_\infty^{(p)}$. Note that decreasing the dimensionless oar length α decreases the stroke duration $T_\infty^{(p)}$ and thus increases the mean injected power.

On the one hand, if one wants to achieve maximum velocity regardless of injected energy—or equivalently mean power—(sprint strategy), one should choose rather short oars $\alpha\sim 1$ (at the limit of the plateau corresponding to the transition between the added mass and pressure drag dominated regimes (figure 7(a1)). However, bear in mind that short oars go hand in hand with high rowing frequency which might be hard to

[8] Note that we here use the parameters of real rowing boats in order to be able to compare our theory to the empirical data.

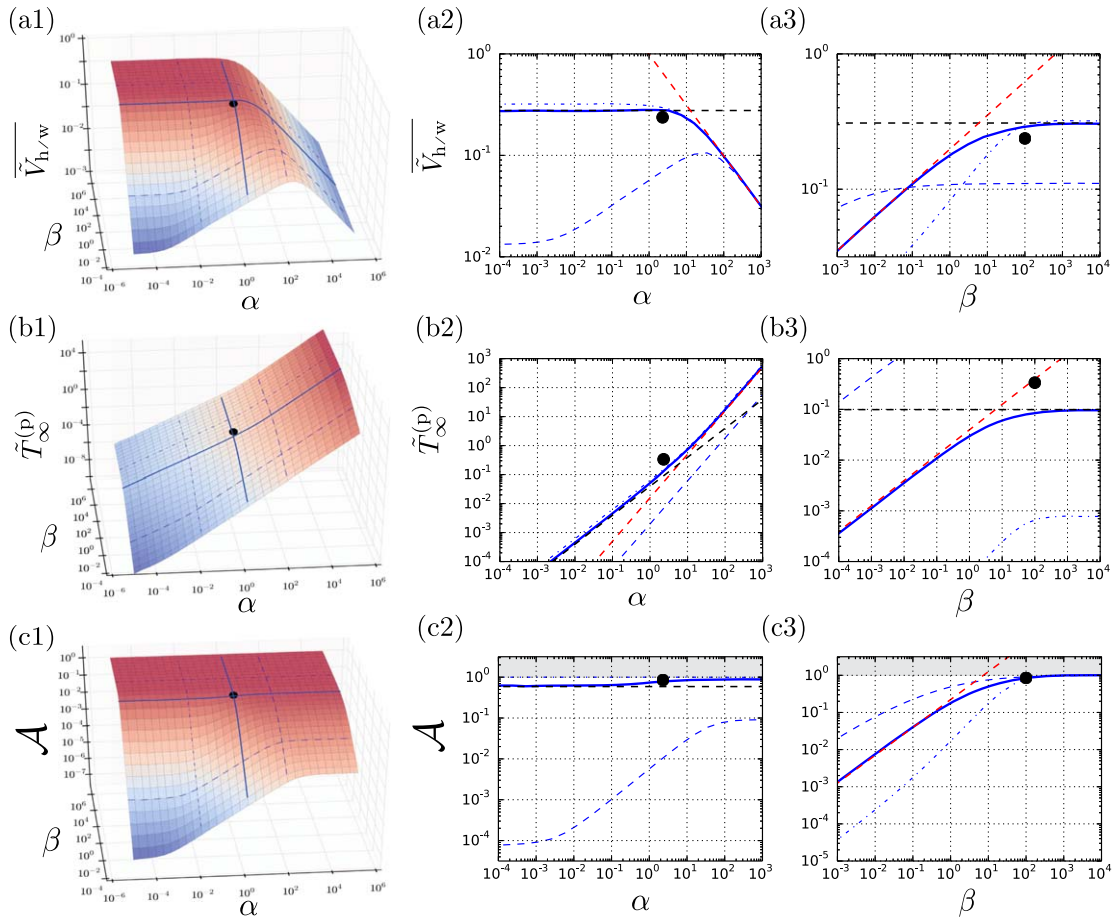

Figure 7. (a1)–(a3) Rescaled mean boat velocity $\overline{\tilde{V}_{\mathrm{h/w}}}$, (b1)–(b3) propulsive stroke duration $\tilde{T}_{\infty}^{(\mathrm{p})}$ and (c1)–(c3) anchoring $\mathcal{A}$ as function of α and β. The manifolds (a1), (b1), (c1) and the curves obtained at given α (a2), (b2), (c2) or given β (a3), (b3), (c3) were obtained numerically with the parameters of a coxless four rowing boat. Asymptotes at small and large scale in (a2), (a3), (b2), (b3), (c2), (c3) are indicated with black and red dashed lines. The black dot in each plot corresponds to the observed data for a coxless four rowing boat.

achieve from a physiological point of view, by that setting a lower bound to α [32, 33]. Furthermore, reducing the oar length imposes to increase the blade surface to maximize the anchoring in water $\mathcal{A}$. On the other hand, if one is rather tempted by maximal efficiency $\mathcal{A} \to 1$ (endurance race), then long oars are indicated in order to reduce the mean power provided by the rower (figure 7(c1)).

Note that all the results presented in figure 7 were obtained for a fixed recovery time $\tilde{T}^{(\mathrm{r})} = 1.1$, roughly corresponding to that of a real rowing race. The recovery time plays a role on the position of the transition point between the different regimes, as well as on the maximal mean velocity $\overline{\tilde{V}_{\mathrm{h/w}}^{\max}}$ reached in the plateau region. Figure 8 displays the maximal mean velocity as function of recovery to propulsion time ratio. Decreasing the recovery time $\tilde{T}^{(\mathrm{r})}$ reduces the fluctuations of the boat velocity and leads to an increasing maximal mean velocity that saturates for $\tilde{T}^{(\mathrm{r})}/T_{\infty}^{(\mathrm{p})} \leqslant 1$. In the limit $\tilde{T}^{(\mathrm{r})}/T_{\infty}^{(\mathrm{p})} \gg 1$, the distance traveled by the boat during the propulsive phase reaches a constant value, while the period of the rowing cycle scales as $\tilde{T}^{(\mathrm{r})}$. Therefore, one has: $\overline{\tilde{V}_{\mathrm{h/w}}^{\max}} \sim 1/\tilde{T}^{(\mathrm{r})}$.

Now, let us focus on the case of a coxless four rowing boat. We consider that each rower deploys a force $F_r = 700$ N (figure 3(a)). The stroke duration, the mean boat velocity and the anchoring computed from our model in this specific case are presented in figure 9. For real sweeping oars, $\alpha \simeq 2.2$ and $\beta \simeq 100$ which lies precisely at the cross-over between the added mass and pressure drag regimes. As one can see in figure 9(c), the estimated anchoring for a coxless four rowing boat [31] compares well with the theoretical anchoring predictions, with $\mathcal{A}$ being close to 80%.

The real mean velocity (figure 9(b)) is smaller than the theoretical one. This is due to all the assumptions of our model: in particular neglecting the effect of the circular motion of the oar, as well as other sources of drag on the hull like the wave drag. Most importantly, the maximal theoretical boat velocity is reached for $\alpha = 0$, while real oars have $\alpha \simeq 2.2$. The stroke duration is also off compared to the theory (figure 9(a)). As mentioned above, physiology imposes a limit to our model. Indeed, the mechanical optima identified here are not always attainable

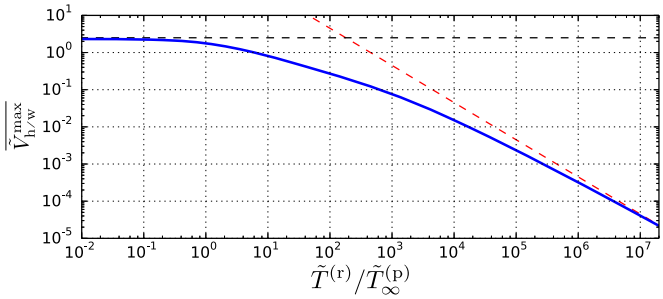

Figure 8. Rescaled maximal mean boat velocity (typically the mean velocity on the plateau, see figure 7(a1)) as function of recovery to propulsion time ratio.

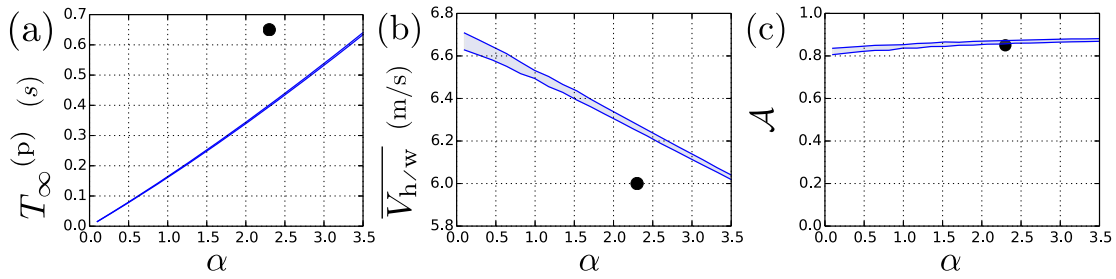

Figure 9. (a) Propulsive stroke duration as function of α. (b) Mean boat velocity as function of α. (c) Anchoring (or equivalently energy transfer efficiency) as function of α (equation (13)). The blue curves were obtained numerically for β between 90 and 120. Empirical data for a coxless four rowing boat are indicated with a black dot.

by the athletes. In particular, the rowers are not able to hold the pace and row at too high frequencies (or equivalently too small stroke durations). A given rower should thus choose the smallest possible oars corresponding to the minimal stroke duration he is able to achieve while deploying a maximal force.

In addition, there is a physiological relationship between the force exerted by a muscle and its characteristic speed, as shown by Hill [32–34]. When the speed increases the force decreases, implying that there exists an optimum power developed by the muscle. In the specific case of rowing, the movement is quite complex and involves a lot of different muscle groups. A physiological study would allow to find the optimum for a given athlete and to confront it with the mechanical optimum to choose the oars. In particular, knowing the precise Hill curve for a given athlete would allow to be more quantitative regarding the optimal geometric parameters. Bear in mind, however, that being fully quantitative would require also to account for other features abstracted in our model such as the effects of lift for example.

Other physiological and practical aspects can be important when it comes to the choice of the oar length. With smaller oars, the rower would have to raise much more the hands, which is not optimal to pull the oar. The techniques for the catch (or blade entry in water) and the release (blade going out of water) should also be changed to adapt with the new oars. Furthermore, for a good synchronization between rowers, it is necessary that all the rowers deploy the same force and have the same oar characteristics [25].

5. Concluding remarks

The present study deals with the question of optimal oar characteristics with a constant imposed force to model the rower, in contrast with most previous works which considered imposed kinematics. This assumption closes the mechanical problem, setting the movement of the rower and the stroke duration. Our theoretical model was validated experimentally in static and dynamic using a robot rowing boat at constant force. We distinguish two regimes depending on whether the force on the blade is dominated by added mass or by pressure drag. We found that real rowing lies at the cross-over between these two regimes.

The optimal oar length and blade size depend on the adopted strategy. If one wants to go as fast as possible without paying attention to the energy consumed (sprint strategy), it is better to use short oars and large blades. If one however aims at minimizing the injected mean power (endurance strategy), long oars and small blades are optimal. Note that olympic rowing races correspond rather to the sprint regime (race duration is around 6 min)

and thus the oars should be small while ensuring a reasonable stroke frequency. This is actually the tendency observed historically on rowing (figure 2).

To conclude, let us underline that our study aims at providing the key ingredients to perform the optimization of oar length and blade size for a given rower depending on the rowing category. To be more quantitative, the effect of the oar angle with respect to the direction of motion, the lift on the blade and the wave drag on the hull could be taken into account. A more realistic force profile could also be injected in the dynamical equations, which would then have to be solved numerically. Finally, note that our work can easily be extended to other sports or propulsive mechanisms, such as kayaking, canoeing[9] and swimming [35].

Acknowledgments

We thank Thomas Baroukh, Renan Cuzon, François Gallaire, Emmanuel Hoang, Kevin Lippera, Hugo Maciejewski and Marc Rabaud for fruitful discussions. We also thank Augustin Mouterde, and Edouard Jonville for providing the handle force data.

Appendix. Single oar dynamics at constant force

Here we derive the dynamics of a single oar at constant force in an immobile hull. We introduce a new velocity scale $V_c = \sqrt{2F_c/(\rho S C_d)}$ and a new time scale $\tau_c = C_m \Omega \sqrt{2\rho/(F_c S C_d)}$ and write: $V = \hat{V} V_c$, $t = \hat{t}\tau_c$ and $F = \tilde{F} F_c$, with F_c the characteristic force introduced in section 4.2. The natural characteristic length of the problem $L_c = V_c \tau_c = 2C_m \Omega/(SC_d)$ compares the effects of added mass and pressure drag. Using equations (3*b*) and (4), one obtains:

$$|\hat{V}_{b/w}|\hat{V}_{b/w} + \dot{\hat{V}}_{b/w} = -\frac{1}{\alpha}\tilde{F}_r. \tag{A.1}$$

Equation (A.1) can be solved numerically for any force profile $\tilde{F}_r(t)$, such that one can determine the exact blade velocity $\hat{V}_{b/w}$.

Letting the deployed force of the rower $F_r = F_c$, namely $\tilde{F}_r = 1$ into equation (A.1), together with $\hat{V}_{b/w}(0) = 0$ yields:

$$\hat{V}_{b/w}(\hat{t}) = -\frac{1}{\sqrt{\alpha}} \tanh\left(\frac{\hat{t}}{\sqrt{\alpha}}\right). \tag{A.2}$$

In particular, one has $\hat{V}_{b/w}(\hat{t} \ll 1) = -\hat{t}/\alpha$ and $\hat{V}_{b/w}(\hat{t} \gg 1) = -1/\sqrt{\alpha}$.

To check equation (A.2) experimentally, we performed a simple experiment involving one oar subjected to a constant force (figure A1(a)). The force was exerted by a reference mass m suspended to a nylon string, itself connected to the oar handle through a pulley (so that $F_r = mg$ where g denotes the acceleration of gravity). The rowlock was attached to the basin boundary. A top view image is presented in figure A1(b). For a given mass m we measured the velocity of the blade while varying $L = 5$–30 cm at constant $\ell = 3$ cm (which amounts to varying α). The blade dimensions were $\ell_b = 7.0$ cm and $h_b = 4.7$ cm. Fitting the theory (equation (A.2)) to the experimental results (figure A1(d)) led to $C_d = 2.0 \pm 0.2$ and $C_m = 0.7 \pm 0.1$ in good agreement with literature values (for a plate of ratio height to span around 0.6, one has $C_d \simeq 1.2$ [36] and $C_m \simeq 0.70$ [37]).

To go one step further, we compute the stroke duration $T^{(p)}$. The travel of the oar end (held by the rower hands) is given by $\Lambda = \theta_0 \ell$ where $\theta_0 = 90°$ (figure 6). The stroke duration $T^{(p)}$ solves:

$$\int_0^{T^{(p)}} V_{r/h}\,dt = \Lambda. \tag{A.3}$$

Note that in the setup working at constant force F_r amounts to working at constant rower energy over a cycle $E_r = \Lambda F_r$. Using equation (A.2), one obtains:

$$T^{(p)} = \tau_c \sqrt{\alpha}\ \cosh^{-1} e^{\alpha\Lambda/L_c}. \tag{A.4}$$

Note that $\alpha\,\Lambda/L_c$ is the dimensionless number that compares the travel of the blade $\alpha\Lambda$ and the characteristic length L_c. As such L_c can be interpreted as the length above which the limit velocity is reached and added mass no longer plays a role. Figure A1(c) displays the theoretical rescaled stroke duration as function of $\alpha\Lambda/L_c$ as well as the experimental data points. The stroke duration increases with α, consistent with increasing blade travel $\alpha\,\Lambda$

[9] In kayaking, as there is no rowlock, $\alpha = 1$, and the stroke frequency observed in competitions is much higher than that of rowing (near 100 strokes per minute), which follows the tendency that the stroke frequency decreases with α (figure 7(b3)). Kayak blades have another specific feature: they are very hollow to increase added mass. However, in comparison with rowing, sprint kayaks tend to go slower as only the rower's arms work (as opposed to legs, back and arms in rowing).

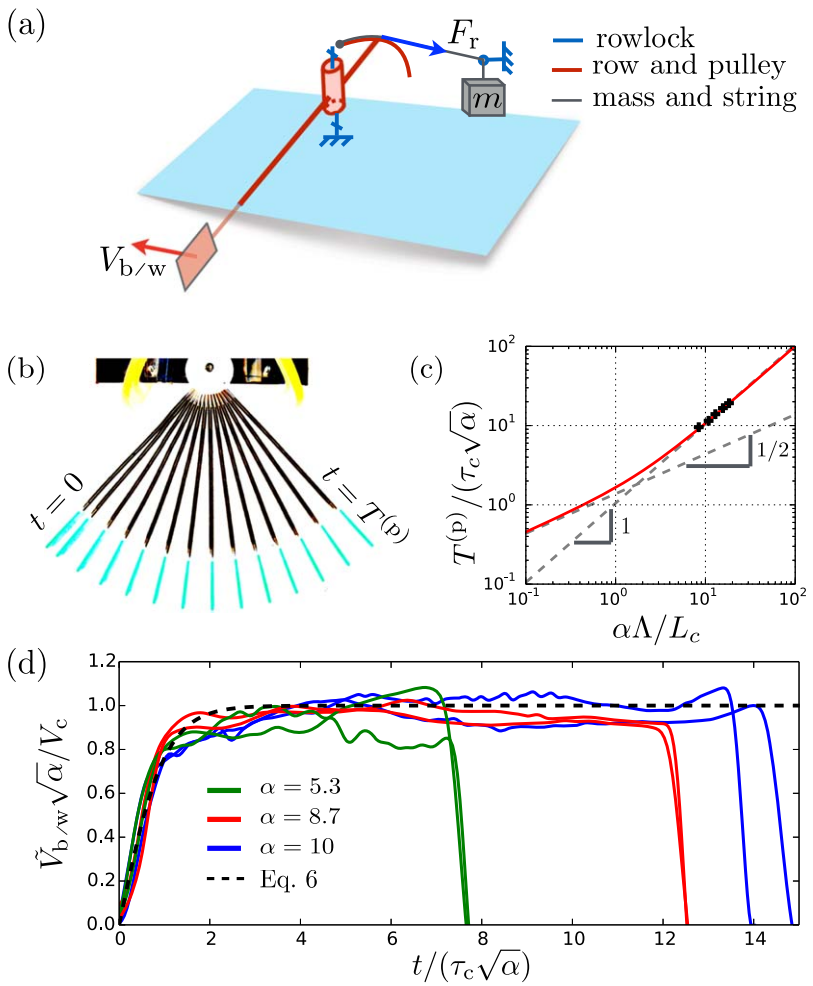

Figure A1. (a) Sketch of the mechanism for the static boat experiment. The oar and pulley (red) rotate with respect to the rowlock (blue) which is fixed in the reference frame of the lab. A suspended mass/string system (gray) ensures oar motion at constant force. (b) Chronophotography of the static boat experiment with a 20 cm oar (corresponding to $\alpha = 5.3$). The time between each frame is 60 ms. (c) Rescaled stroke duration as function of rescaled stroke length. The red curve corresponds to equation (A.4) and the black crosses signify experimental data with constant $F_0 = 5$ N while varying α. (d) Dimensionless velocity as function of dimensionless time for three different values of α, each with two values of $F_0 \in \{5\text{ N}, 10\text{ N}\}$.

and decreasing blade propulsive force F_r/α. Decreasing α amounts to increasing rowing frequency. Two regimes can be distinguished: an added mass dominated regime corresponding to $\alpha\Lambda/L_c \ll 1$ for which $T^{(p)} \sim \alpha$, and a pressure drag dominated phase for which $\alpha\Lambda/L_c \gg 1$ and $T^{(p)} \sim \alpha^{3/2}$ (note that the experimental data on figure A1(c) lies on the pressure drag dominated phase).

ORCID iDs

Michael Benzaquen https://orcid.org/0000-0002-9751-7625

References

[1] McArthur J 1997 *High Performance Rowing* (Ramsbury: Crowood Press)
[2] Nolte V 2005 *Rowing Faster* vol 1 (Location: Champaign, IL: Human Kinetics)
[3] http://concept2.com/oars/oar-options/length (Accessed: 02 April 2019)
[4] Nilson T S, Daigneault T and Smith M 1987 *The FISA Coaching Development Programme Course, Handbook—Level III* (Lausanne: FISA)
[5] https://en.wikipedia.org/wiki/Oar_(sport_rowing) (Accessed: 02 April 2019)
[6] Nolte V 2009 Shorter oars are more effective *J. Appl. Biomech.* **25** 1–8
[7] https://en.wikipedia.org/wiki/List_of_The_Boat_Race_results (Accessed: 02 April 2019)
[8] http://worldrowing.com/ (Accessed: 11 October 2018)
[9] Kleshnev V 2016 *Biomechanics of Rowing* (Ramsbury: Crowood Press)
[10] http://biorow.com/ (Accessed: 02 April 2019)
[11] Wellicome J 1967 Report on resistance experiments carried out on three racing shells *Natl Phys. Lab. Ship TM* **184** 1
[12] Day A, Campbell I, Clelland D, Doctors L J and Cichowicz J 2011 Realistic evaluation of hull performance for rowing shells, canoes, and kayaks in unsteady flow *J. Sports Sci.* **29** 1059–69

[13] Caplan N, Coppel A and Gardner T 2010 A review of propulsive mechanisms in rowing *Proc. Inst. Mech. Eng.* P **224** 1–8
[14] Grift E J, Vijayaragavan N B, Tummers M J and Westerweel J 2019 Drag force on an accelerating submerged plate *J. Fluid Mech.* **866** 369–98
[15] Barré S and Kobus J 2010 Comparison between common models of forces on oar blades and forces measured by towing tank tests *Proc. Inst. Mech. Eng.* P **224** 37–50
[16] Caplan N and Gardner T N 2007 A fluid dynamic investigation of the big blade and macon oar blade designs in rowing propulsion *J. Sports Sci.* **25** 643–50
[17] Laschowski B, Hopkins C C, de Bruyn J R and Nolte V 2017 Modelling the deflection of rowing oar shafts *Sports Biomech.* **16** 76–86
[18] Lintmeijer L L, Onneweer J P, Hofmijster M J, Wijgergangs W A, De Koning H, Clairbois B, Westerweel J, Grift E J, Tummers M J and Van Soest A 2019 Towards determination of power loss at a rowing blade: validation of a new method to estimate blade force characteristics *PLoS One* **14** e0215674
[19] Sliasas A and Tullis S 2011 Modelling the effect of oar shaft bending during the rowing stroke *Proc. Inst. Mech. Eng.* P **225** 265–70
[20] Alexander F 1925 The theory of rowing *Proc. University of Durham Philosophical Society* vol 6
[21] Cabrera D, Ruina A and Kleshnev V 2006 A simple 1+ dimensional model of rowing mimics observed forces and motions *Hum. Mov. Sci.* **25** 192–220
[22] Laschowski B, Nolte V, Adamovsky M and Alexander R 2015 The effects of oar-shaft stiffness and length on rowing biomechanics *Proc. Inst. Mech. Eng.* P **229** 239–47
[23] Vespoli M, Nelson B and Scragg C 1995 Eight man rowing shell *US Patent* 5,474,008
[24] Boucher J, Labbé R and Clanet C 2017 Row bots *Phys. Today* **70** 82–3
[25] Leroyer A, Barré S, Kobus J-M and Visonneau M 2008 Experimental and numerical investigationsof the ow around an oar blade *J. Mar. Sci. Technol.* **13** 1–15
[26] Baudouin A and Hawkins D 2002 A biomechanical review of factors affecting rowing performance *Br. J. Sports Med.* **36** 396–402
[27] Caplan N and Gardner T N 2007 A fluid dynamic investigation of the big blade and macon oar blade designs in rowing propulsion *J. Sports Sci.* **25** 643–50
[28] Baudouin A and Hawkins D 2004 Investigation of biomechanical factors affecting rowing performance *J. Biomech.* **37** 969–76
[29] Jones C and Miller C 2002 The mechanics and biomechanics of rowing *Coaching Forum Meeting at York City Rowing Club*
[30] McMahon T 1971 Rowing: a similarity analysis *Science* **173** 349–51
[31] Kleshnev V 1999 Propulsive efficiency of rowing *ISBS-Conf. Proc. Archive* vol 1
[32] Hill A V 1938 The heat of shortening and the dynamic constants of muscle *Proc. R. Soc.* B **126** 136–95
[33] Wilkie D 1949 The relation between force and velocity in human muscle *J. Physiol.* **110** 249–80
[34] Cohen C, Texier B D, Laffaye G, Auvray L and Clanet C 2015 Weightlifting and the actomyosin cycle *Proc. R. Soc.* A **471** 20150473
[35] Pendergast D, Zamparo P, Di Prampero P, Capelli C, Cerretelli P, Termin A, Craig A, Bushnell D, Paschke D and Mollendorf J 2003 Energy balance of human locomotion in water *Eur. J. Appl. Physiol.* **90** 377–86
[36] Hoerner S F 1965 *Fluid-Dynamic Drag: Practical Information on Aerodynamic Drag and Hydrodynamic Resistance* (Hoerner Fluid Dynamics)
[37] Blevins R D and Plunkett R 1980 Formulas for natural frequency and mode shape *J. Appl. Mech.* **47** 461